Commun. Comput. Phys.
doi: 10.4208/cicp.170612.240113a

Vol. **14**, No. 4, pp. 1058-1072
October 2013

Pressure Distribution of the Gaseous Flow in Microchannel: A Lattice Boltzmann Study

Zimian Xu and Zhaoli Guo*

State Key Laboratory of Coal Combustion, Huazhong University of Science and Technology, Wuhan 430074, Hubei, China.

Received 17 June 2012; Accepted (in revised version) 24 January 2013

Communicated by Kazuo Aoki

Available online 8 May 2013

Abstract. In this paper the pressure distribution of the gaseous flow in a microchannel is studied via a lattice Boltzmann equation (LBE) method. With effective relaxation times and a generalized second order slip boundary condition, the LBE can be used to simulate rarefied gas flows from slip to transition regimes. The Knudsen minimum phenomena of mass flow rate in the pressure driven flow is also investigated. The effects of Knudsen number (rarefaction effect), pressure ratio and aspect ratio (compression effect) on the pressure distribution are analyzed. It is found the rarefaction effect tends to the curvature of the nonlinear pressure distribution, while the compression effect tends to enhance its nonlinearity. The combined effects lead to a local minimum of the pressure deviation. Furthermore, it is also found that the relationship between the pressure deviation and the aspect ratio follows a pow-law.

AMS subject classifications: 76P05

Key words: Lattice Boltzmann method, gaseous flows, pressure distribution, microchannel.

1 Introduction

Pressure driven gaseous flows in microchannels are getting more attention nowadays due to their key role in the Micro-Electro-Mechanical-System (MEMS) [1–3]. Usually, a microchannel flow is characterized by the Knudsen number $\mathrm{Kn}=\lambda/L$, where λ is the mean-free-path (MFP) of the gas and L is the channel height. According to the value of Kn, the flow can be classified into four types, i.e., continuum flow $(\mathrm{Kn}<0.001)$, slip flow $(0.001\leq\mathrm{Kn}<0.1)$, transition flow $(0.1\leq\mathrm{Kn}<10)$, and free-molecular flow $(\mathrm{Kn}\geq 10)$. In such flows, the gas density changes along the channel and Kn vary in a wide range for

*Corresponding author. *Email addresses:* xzmmzx@gmail.com (Z. M. Xu), zlguo@mail.hust.edu.cn (Z. L. Guo)

a long channel. Consequently, it is rather a challenging task to simulate such multi-scale flows.

Previously, a variety of studies have been conducted to simulate gaseous flows in microchannels using different methods. Arkilic et al. obtained an analytical solution of the pressure driven flows in long channels based on the compressible Navier-Stokes (N-S) equations with a first-order slip boundary condition [4]. Jang et al. gained a more accurate analytical solution by considering the geometry and temperature [5]. Since the N-S equations together with the slip boundary condition do not work beyond the slip regime, the results are only valid for slip flows. Shen et al. applied the Information-Preservation Direct Simulation Monte Carlo (IP-DSMC) method to simulate the microchannel flows in both slip and transitional regimes, where the mass flow and pressure distribution were reported [6]. Maurer et al. investigated the effect of the slip coefficient on the slip regime based on the N-S equations with a second order slip boundary condition [7]. Varoutis et al. presented some computations by lattice Boltzmann equation (LBE) and experimental results of the gaseous flows through long channels with triangular and trapezoidal cross sections [8]. On the other hand, Ohwada et al. explored the channel flow [9] by solving the linearized Boltzmann equation under the assumption of small pressure gradient.

However, most of the available studies concentrate on the gas velocities and mass flow rates, and very few attention has been paid to the distribution of pressure under different conditions. Due to the combined rarefaction and compression effects in microscale gaseous flows, the pressure distribution in the channel is usually nonlinear. In this work, we will focus on this topic to understand how the pressure distribution is influenced by the flow parameters.

The rest of the paper is organized as follows. The physical problem is described in Section 2, and in Section 3 we briefly introduce the numerical method. Numerical results and discussions are then provided in Section 4, and finally a summary is given in Section 5.

2 Problem description

The problem considered is a pressure-driven gas flow in a two-dimensional (2D) microchannel with length L and height H as shown in Fig. 1, two walls locate at $y=0$ and $y=H$, respectively. The aspect ratio is defined as $\varepsilon=H/L$. The pressure at the inlet and outlet are fixed at P_{in} and P_{out}, respectively, and the pressure ratio is denoted by $\theta_p=P_{in}/P_{out}$.

In slip regime, the flow can be described by the compressible Navier-Stokes equations, supplemented by a slip velocity,

$$u_{wall}=\frac{\sigma-2}{\sigma}\mathrm{Kn}\frac{\partial u}{\partial y}\Big|_{wall}, \tag{2.1}$$

where u is the tangential velocity, y is the spanwise direction, σ is the tangential momentum accommodation. Arkilic et al. [4] solved the governing equations with a perturbation

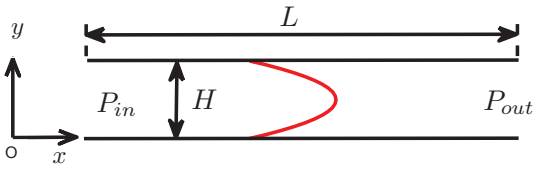

Figure 1: Pressure driven gas flow in a channel.

method under the assumption that $\varepsilon \ll 1$ and $T = constant$. The nondimensional pressure distributions is,

$$\widetilde{p}(\widetilde{x}) = -6\sigma \mathrm{Kn} + \sqrt{(6\sigma \mathrm{Kn})^2 + (1+12\sigma \mathrm{Kn})\widetilde{x} + (\theta_p^2 + 12\sigma \mathrm{Kn}\theta_p)(1-\widetilde{x})}, \tag{2.2}$$

where $\tilde{p} = P/P_{out}$, $\tilde{x} = x/L$, the dimensionless streamwise and spanwise velocity components $\tilde{u}$ and $\tilde{v}$ are

$$\tilde{u} = -\frac{\epsilon R}{8\gamma Ma^2}\frac{d\widetilde{p}}{d\tilde{x}}\left(1 - 4\tilde{y}^2 + 4\sigma\frac{\mathrm{Kn}_{out}}{\widetilde{p}}\right), \tag{2.3a}$$

$$\tilde{v} = \frac{\epsilon R}{8\gamma Ma^2}\frac{1}{\widetilde{p}}\left[\frac{1}{2}\frac{d^2(\widetilde{p}^2)}{d\tilde{x}^2}\left(\tilde{y} - \frac{4}{3}\tilde{y}^3\right) + 4\sigma \mathrm{Kn}_{out}\tilde{y}\frac{d^2\widetilde{p}}{d\tilde{x}^2}\right], \tag{2.3b}$$

where $\tilde{u} = u/u_{out}$ and $\tilde{v} = v/v_{out}$, u and v are the velocities at streamwise and spanwise, respectively, u_{out} and v_{out} are the average velocities at channel exit. It should be noted that the non-zero spanwise velocity is due to the compressibility effect [10]. In this problem, Jang et al. obtained a more accurate solution under negligible transverse velocities with a first order slip boundary condition. The pressure distribution is given by [5]:

$$\widetilde{p}(\widetilde{x}) = -\mathrm{Kn}C + \sqrt{\mathrm{Kn}C^2 + 1 + 2\mathrm{Kn}C + [\theta_p^2 - 1 + 2\mathrm{Kn}C(\theta_p - 1)](1-\widetilde{x})}, \tag{2.4}$$

where C is

$$C = P_{out}^2 + 2\frac{2-\sigma}{\sigma}\mathrm{Kn}_{out}\frac{\alpha_2}{\alpha_1} + \frac{2mR_sT\mu(x-L)}{w_cH^3\alpha_1}, \tag{2.5}$$

α_1 and α_2 are two parameters dependent on the channel geometry, R_s is the gas constant, T is the temperature, x is the streamwise coordinate, and μ is the viscosity of the gas.

From the above results, we can see that even in the slip regime, the pressure distribution and the velocity fields are highly nonlinear functions of a number of parameters such as Kn and θ_p.

3 Numerical method: lattice Boltzmann equation

3.1 LBE model

We will employ the LBE method to simulate the micro gas flow described above. Actually, the LBE method has been employed to simulate microscale gas flows by a number

of researchers. For instance, Nie et al. [11] studied the microchannel gas flow as Kn ranges from 0.0194 to 0.776, and the nonlinear pressure distribution was reported. Verhaeghe et al. [10] studied the microchannel flow with a multiple relaxation time (MRT) LBE together with a first-order slip boundary condition, and reproduced the velocity and pressure fields that were consistent with the analytical solutions in [4]. Lim et al. applied the LBE method to the two-dimensional pressure driven microchannel flow in slip regime [12], and Zhang et al. simulated low speed slip flows [13]. In the above applications, the LBE models employed are for solving the Navier-Stokes equations, which are not applicable for flows with large Knudsen numbers. In order to simulate flows in the transition regime, some improved LBE models in which the Knudsen layer (KL) effects are incorporated have been developed [14]. For instance, Guo et al. [15] proposed an LBE model with an effective relaxation time which includes the KL effects, and they simulated the microchannel flow with Knudsen number up to 0.388. Later a MRT-LBE with a local effective relaxation time was further developed [16], which was found to be able to give good predictions of the force-driven microchannel flow from slip to transition regimes.

In our simulations we will employ MRT-LBE developed by Guo et al. [15, 16]. The evolution equations of this model can be expressed as

$$Collison: \quad f_i'(\mathbf{x},t) = f_i(\mathbf{x},t) - \mathbf{\Lambda_{ij}}[f_j - f_j^{eq}], \quad i = 0,1,2,\cdots,b-1, \tag{3.1a}$$

$$Streaming: \quad f_i(\mathbf{x}+\mathbf{c}_i\Delta t, t+\Delta t) = f_i'(\mathbf{x},t), \tag{3.1b}$$

where f_i is the distribution function, $\mathbf{x}$ is the position, t is the time, $\mathbf{c}_i$ is the discrete velocities, b is the total number of the directions, $\mathbf{\Lambda_{ij}}$ is the collision matrix, f_i^{eq} is the equilibrium distribution function, and Δt is the time step length. The collision process of MRT-LBE is implemented in the moment space, the moments are defined as

$$\mathbf{m} = \mathbf{M}\mathbf{f}, \tag{3.2}$$

where $\mathbf{f} = (f_0, f_1, \cdots, f_{b-1})^T$ is the distribution function in moment-space, $\mathbf{M}$ is the projection matrix. The collision in moment-space is

$$\mathbf{m}' = \mathbf{m} - \mathbf{S}[\mathbf{m} - \mathbf{m}^{(eq)}], \tag{3.3}$$

where $\mathbf{m}'$ is the post-collision moments corresponding to $f_i'(\mathbf{x},t)$, and $\mathbf{S} = \mathbf{M}\mathbf{\Lambda}\mathbf{M}^{-1} = diag(\tau_0, \tau_1, \cdots, \tau_{b-1})^{-1}$ is the relaxation rate diagonal matrix. $\mathbf{m}^{(eq)}$ are the equilibrium moments defined as

$$\mathbf{m}^{(eq)} = \mathbf{M}f^{(eq)}. \tag{3.4}$$

After the collision step (Eq. (3.3)), the standard streaming step can be executed after transforming back to the velocity space, $f_i'(x,t) = \mathbf{M}_{i,j}^{-1}\mathbf{m}_{i,j}'$. The fluid density ρ and velocity $\mathbf{u}$ are defined respectively as

$$\rho = \sum f_i, \quad \mathbf{u} = \sum \mathbf{c}_i f_i / \rho. \tag{3.5}$$

In this work we consider the two-dimensional nine-velocity lattice model (D2Q9), the equilibrium distribution function in Eq. (3.1) can be expressed as

$$f_i^{eq}=\omega_i\rho\left[1+\frac{\mathbf{c}_i\cdot\mathbf{u}}{c_s^2}+\frac{(\mathbf{c}_i\cdot\mathbf{u})^2}{2c_s^4}-\frac{\mathbf{u}\cdot\mathbf{u}}{2c_s^2}\right], \tag{3.6}$$

where $\omega_0=4/9$, $\omega_i=1/9(i=1-4)$, $\omega_i=1/36(i=5-8)$, $c_s^2=1/3$, and $\mathbf{c}_i$ is defined as

$$\mathbf{c_i}=\begin{cases}(0,0), & i=0,\\ \big(\cos[(i-1)\pi/2],\sin[(i-1)\pi/2]\big)c, & i=1-4,\\ \big(\cos[(2i-9)\pi/4],\sin[(2i-9)\pi/4]\big)\sqrt{2}c, & i=5-8,\end{cases} \tag{3.7}$$

where $c=\delta x/\delta t$, δx and δt are the lattice spacing and time step, respectively, and the transform matrix $\mathbf{M}$ is given as

$$\mathbf{M}=\begin{pmatrix}1&1&1&1&1&1&1&1&1\\-4&-1&-1&-1&-1&2&2&2&2\\4&-2&-2&-2&-2&1&1&1&1\\0&1&0&-1&0&1&-1&-1&1\\0&-2&0&2&0&1&-1&-1&1\\0&0&1&0&-1&1&1&-1&-1\\0&0&-2&0&2&1&1&-1&-1\\0&1&-1&1&-1&0&0&0&0\\0&0&0&0&0&1&-1&1&-1\end{pmatrix}. \tag{3.8}$$

The corresponding discrete velocity moments are

$$\mathbf{m}=\big(\rho,e,\varepsilon,j_x,q_x,j_y,q_y,p_{xx},p_{xy}\big)^T, \tag{3.9}$$

and the relaxation matrix corresponding to the nine moments is given by

$$\mathbf{S}=diag\big(\tau_\rho,\tau_e,\tau_\varepsilon,\tau_d,\tau_q,\tau_d,\tau_q,\tau_s,\tau_s\big)^{-1}. \tag{3.10}$$

Through the Chapman-Enskog analysis, we can derive the hydrodynamic equations where the kinematic and bulk viscosities are

$$\nu=c_s^2\Big(\tau_s-\frac{1}{2}\Big)\delta_t,\quad \zeta=c_s^2\Big(\tau_e-\frac{1}{2}\Big)\delta_t. \tag{3.11}$$

3.2 Effective Knudsen number and relaxation time

As a gas flows over a solid wall, a Knudsen Layer (KL) with thickness of the order of the mean-free-path will appear. Within the KL, the quasithermodynamic-equilibrium assumption breaks down. Consequently, the standard LBE, which is only accurate at the

Navier-Stokes level as an approximation to the Boltzmann equation, will fail in describing the KL [18–22]. In order to capture the flow in KL using LBE, two approaches can be employed. The first one is to use some high-order models [26] which approximate the full Boltzmann equation at higher levels than the Navier-Stokes, and the second approach is to extend the standard LBE by incorporating the effects of the KL through some heuristic models [16, 21, 23–25]. Here we adopt the model developed in [16], in which KL effects are considered through an effective mean free path λ_e,

$$\lambda_e = \lambda \Psi(y, \mathrm{Kn}), \tag{3.12}$$

where Ψ is a function that describes the KL effect. In the microchannel flow where the two parallel plates locate at $y=0$ and $y=H$, it was suggested that [16]

$$\Psi(y) = \frac{1}{2}\left[\psi\left(\frac{y}{H}\right) + \psi\left(\frac{H-y}{H}\right)\right], \tag{3.13}$$

where

$$\psi(\alpha) = 1 + (\alpha - 1)e^{-\alpha} - \alpha^2 E_i(\alpha), \tag{3.14}$$

E_i is the exponential integral function, $E_i(x) = \int_1^\infty t^{-1} e^{-xt} dt$. From the effective mean-free-path, we can obtain the effective Knudsen number,

$$\mathrm{Kn}_e = \mathrm{Kn}\Psi, \tag{3.15}$$

on the other hand, from kinetic theory we know that the MFP is related to the kinematic viscosity [17],

$$\lambda = \frac{\mu}{p}\sqrt{\frac{\pi RT}{2}}. \tag{3.16}$$

Therefore, if we assume this relationship also holds for the effective mean-free-path, we can define an effective relaxation time τ_s as [16],

$$\tau_s = \frac{1}{2} + \sqrt{\frac{6}{\pi}} N \mathrm{Kn} \Psi(y, Kn), \tag{3.17}$$

where $N = H/\delta x$.

3.3 Kinetic boundary condition

A suitable slip boundary condition should be provided to study microscale gaseous flows. For flows in slip regime, a number of first-order and second-order slip boundary conditions have been developed [17, 27–32], and some schemes to realize these boundary conditions in LBE have been constructed [33, 34]. For flows in transition regime, Guo et al. proposed a generalized second-order slip boundary condition [16]

$$U_s = A_1\left(\lambda_e \frac{du}{dn}\right)_{wall} - A_2\left[\frac{\lambda_e}{2}\frac{d}{dn}\left(\lambda_e \frac{du}{dn}\right)\right], \tag{3.18}$$

where A_1 and A_2 are given by

$$A_1=\frac{2-\sigma}{\sigma}(1-0.1817\sigma),\quad A_2=\frac{1}{\pi}+\frac{1}{2}A_1^2, \tag{3.19}$$

where $\sigma=1$ is the accommodation coefficient, the wall is fully diffusive. In order to treat this boundary condition in the D2Q9 MRT-LBE, the bounceback-specular-reflection (BSR) scheme is employed:

$$f_2=f_4^{'},\quad f_5=rf_7^{'}+(1-r)f_8^{'},\quad f_6=rf_8^{'}+(1-r)f_7^{'}, \tag{3.20}$$

for the bottom plate, and

$$f_4=f_2^{'},\quad f_7=rf_5^{'}+(1-r)f_6^{'},\quad f_8=rf_6^{'}+(1-r)f_5^{'}, \tag{3.21}$$

for the top plate, where r is a parameter representing the bounce-back portion.

To realize the slip boundary condition (Eq. (3.18)) exactly, the parameter r and the relaxation time τ_q should be chosen as follows [16]:

$$r=\left[1+\varsigma A_1+\frac{\tau_s'(0)\delta_x}{8\widetilde{\tau}_s^2(0)}\right]^{-1}, \tag{3.22a}$$

$$\tau_q=0.5+\frac{3+24\varsigma^2\widetilde{\tau}_s^2(0)A_2}{16\widetilde{\tau}_s(0)}+\frac{\widetilde{\tau}_s'(0)\delta_x[12+30\widetilde{\tau}_s(0)\varsigma A_1]}{16\widetilde{\tau}_s^2(0)}, \tag{3.22b}$$

where $\varsigma=\sqrt{\pi/6}$, $\widetilde{\tau}_s=\tau_s-0.5$, and $\tau_s'=d\tau_s/dy$.

The pressure boundary conditions at the inlet and outlet of the channel should also be correctly implemented in the LBE. It should be noted that the inlet and outlet pressures should be considered as averaged pressures instead of constant ones. Otherwise, the flow field in the channel will be significantly influenced by the end effect. Here we employ an extrapolation-correction technique. At the inlet $(x=0)$, the unknown distribution functions and density are obtained by extrapolation from the inner nodes:

$$f_i(0,j)=2f_i(1,j)-f_i(2,j),\quad \rho^{'}(0,j)=2\rho(1,j)-\rho(2,j), \tag{3.23}$$

where 0, 1 and 2, are the nodes at the inlet, first layer, and second layer, respectively. The density is then corrected so that the average density ρ_{in} matches the averaged pressure,

$$\rho(0,j)=\rho^{'}(0,j)\frac{N\rho_{in}}{\sum\rho^{'}(0,j)}, \tag{3.24}$$

where $\rho_{in}=p_{in}/c_s^2$. The distribution functions and densities at the outlet can be obtained similarly.

It should be emphasized that the LBE method described above are constructed heuristically. In this method the KL effects are incorporated into the relaxation times instead of solving the full Boltzmann equation. This method is able to capture some nontrivial behaviors of transition flows effectively provided a suitable KL model is employed, as demonstrated in [16].

4 Results and discussion

In our simulations the relaxation times τ_s and τ_q are given by Eqs. (3.17) and (3.22b), respectively. The other ones are set as follows: $\tau_\rho = \tau_j = 1$, $\tau_e = 1.1$, and $\tau_\varepsilon = 1.2$. We found that the results are insensitive to the values of these relaxation times. And then, we will focus on the pressure distribution with different outlet Knudsen numbers, pressure ratios, and aspect ratios.

4.1 Validation

First, a comparison study is made to valid the numerical method. The aspect ratio ε is fixed at 0.01, the pressure ratio θ_p is set to be 2.0, and the outlet Knudsen number is fixed at 0.388. In this case the flow is in the transition regime. These parameters were also adopted in some previous works [6, 10]. In simulations, a 10×1000 lattice is employed, which can produce grid-independent results.

Fig. 2 shows the normalized pressure deviation from the linear one, $\Delta P = [P(x,y) - P_l]/P_{out}$ and the normalized streamwise velocity $u/u_{\max}$, where P_l is the linear pressure distribution along the channel and $u_{\max}$ is the maximum streamwise velocity. Previous results [6, 10] are also included for comparison.

As shown in Fig. 2, the velocity profile predicted by the present LBE is in good agreement with those of other methods in the central region. Furthermore, in comparison with the LBE result by Verhaeghe et al. [10], a better agreement with the DSMC and IP-DSMC results is observed in the near wall regions where the KL effects are significant. Regarding the nonlinear pressure deviation, the present MRT-LBE produces a better prediction than the method used by Verhaeghe et al. [10] in comparison with the results of the DSMC and IP-DSMC methods.

We also simulated the flow with other Knudsen numbers. For a quantitative compari-

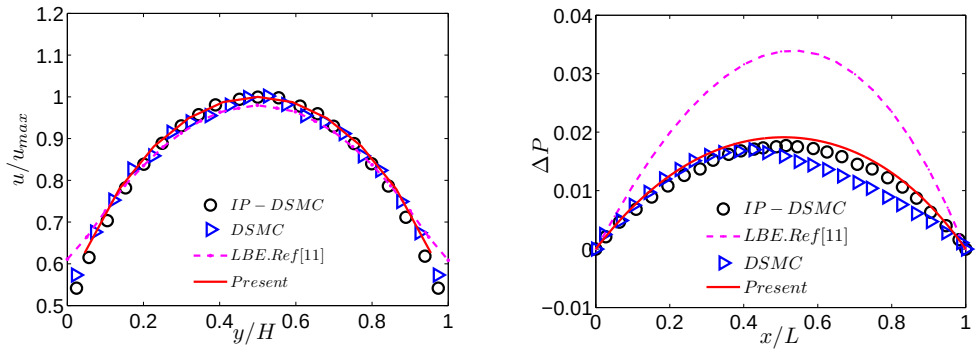

(a) (b)

Figure 2: Streamwise velocity (a) and pressure deviation (b) of the present LBE and those of other methods. $\mathrm{Kn}_{\mathrm{out}} = 0.388$ and $\theta_p = 2.0$.

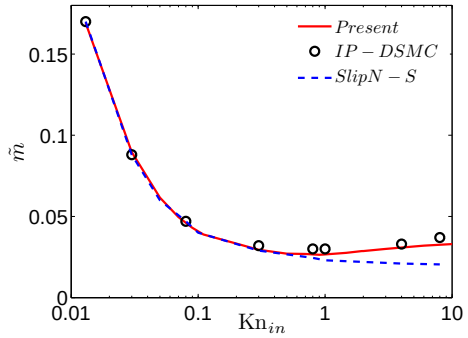

Figure 3: Normalized mass flow rate function of the Knudsen number at the inlet ($\mathrm{Kn}_{\mathrm{in}}$), the IP-DSMC Date are taken from [35].

son, the flow conditions in our simulations are similar to those used in [35]. Specially, the aspect ratio is 1/20 and the pressure ratio is set to be 10/7. We measured the normalized mass flow defined as follow [35]:

$$\tilde{m} = \rho u H / (\rho_{avg} \sqrt{2RT}), \tag{4.1}$$

where ρ_{avg} is defined as $(\rho_{in}+\rho_{out})/2$. The results are shown in Fig. 3. For comparison, the results of the Navier-Stokes method, and the IP-DSMC are presented [35]. It is observed that the Knudsen minimum phenomenon of mass flow rate is successfully captured by the present LBE and the IP-DSMC methods, and both results match well up to $\mathrm{Kn} = 10$. However, the Navier-Stokes solutions deviate from the IP data as $\mathrm{Kn} \geq 1$. The above results confirm that the present LBE has the capability of simulating microscale gas flows ranging from continuum to transition regimes.

4.2 Effects of pressure ratio and Knudsen number

Now we consider the flows under different pressure ratios and Knudsen numbers. The compression effect (pressure ratio) and rarefaction effect (Knudsen number) have significant combined influence on the pressure distribution of the microscale flow. The values of Kn_{out} are set to be 0.025, 0.1, 1.0, and 10, respectively, so that the flows range from the slip to transition regimes. The values of θ_p range from 2.0 to 7.0.

The normalized pressure distributions are presented in Fig. 4. It is first observed that the nonlinearity of the pressure deviation decreases with increasing Kn, and pressure distributions are almost linear at different pressure ratios as the Knudsen number is large ($\mathrm{Kn}_{out} = 1$ and 10), on the other hand, the pressure distributions are obvious nonlinear as $\mathrm{Kn}_{out} = 0.1$. Such phenomenon is consistent with previous experiment results [8].

To further investigate the rarefaction effect on the nonlinearity of the pressure distribution, we now focus on the cases of $\theta_p = 3.0$ and 6.0. The pressure deviations at different Kn_{out} are shown in Fig. 5(a). It can be seen in the figure that when $\theta_p = 3.0$ ΔP decreases with increasing Kn_{out} as $\mathrm{Kn}_{out} \leq 1$, and falls below zero as $\mathrm{Kn}_{out} > 1$. This is because that

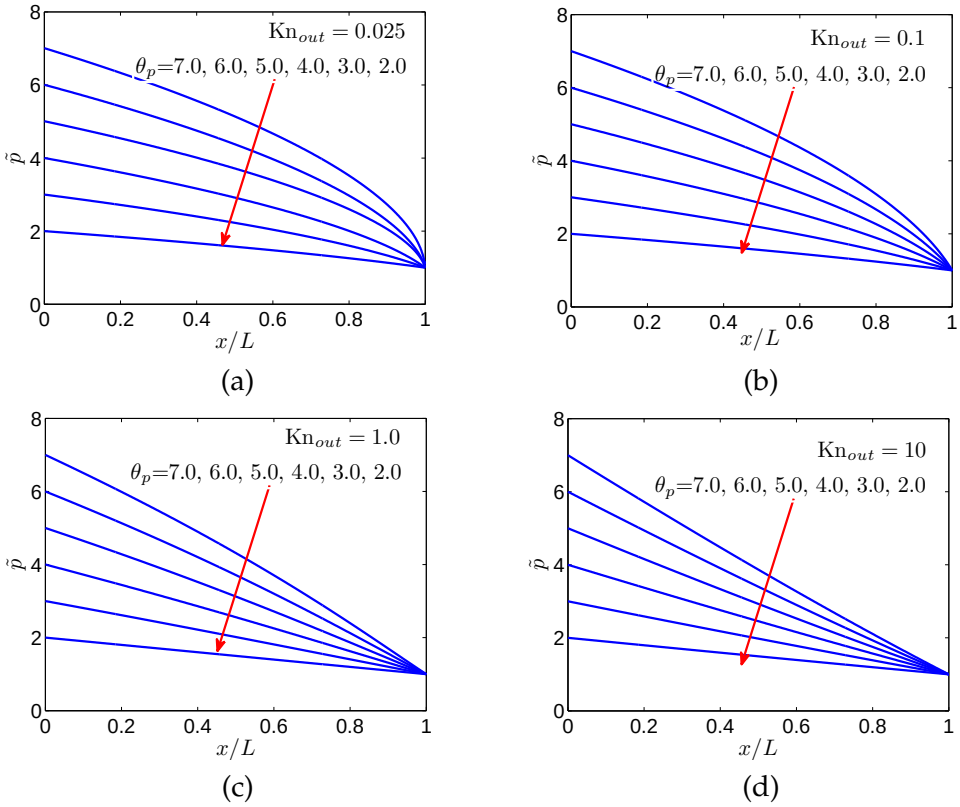

Figure 4: Pressure distribution with different θ_p and Kn$_{out}$.

the rarefaction effect is enhanced when Kn$_{out}$ increases, and the loss of pressure would be faster than that with a lower Kn$_{out}$. However, ΔP increases as Kn$_{out} \geq 5$, which indicates that the rarefication effect is limited. Therefore, there will be a minimum in ΔP as Kn$_{out}$ increase from 1 to 10. The change of the pressure distributions,

$$\|\Delta P\| = \frac{1}{N}\left(\sum_{i=1}^{N} \Delta P_i\right)$$

is measured for each case and the results are shown in Fig. 5(b). A minimum at Kn$_{out} \approx 4$ is clearly demonstrated for $\theta_p = 3.0$, which is similar to the "Knudsen minimum" in the mass flow rate (see Fig. 3). It is also noted that as θ_p=6.0, the minimum occurs at Kn$_{out} \approx 6$, which is greater than that as $\theta_p = 3.0$. This is because the compression effect at $\theta_p = 6.0$ is more significant, and a larger rarefaction effect is required to balance it at the minimum point.

Fig. 4 also shows that the nonlinear pressure distribution is a function of the pressure ratio. This can be seen more clearly in Fig. 6, in which Fig. 6(a) gives the $\tilde{p}$ in the same channel but with different θ_p and downstream pressures. It can be observed that the difference in the pressure has no effect on the normalized pressure distribution. We can find

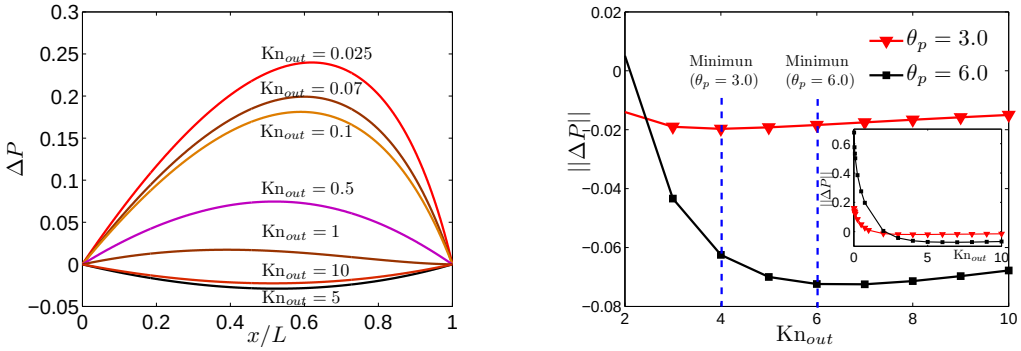

Figure 5: (a): ΔP along the channel with $\theta_p=3.0$ and different Kn_{out}. (b): Pressure deviations along the channel as $\theta_p=3.0$ and 6.0.

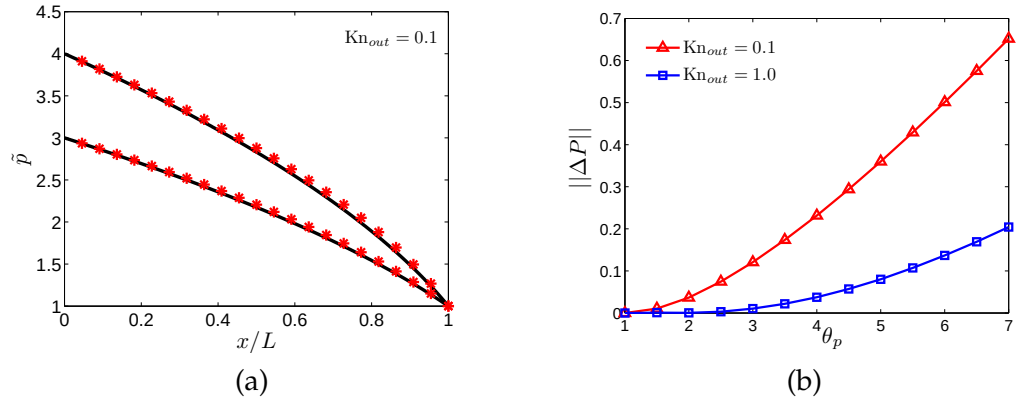

Figure 6: Pressure distribution with different θ_p. (a): ε=0.01, θ_p=3:1,4:1,6:2,8:2. The asterisk is the pressure distribution when downstream pressure is 2.0. (b): $\|\Delta P\|$ with different θ_p.

in Fig. 6 that in the slip regime (Kn_{out}=0.1) the increase of θ_p leads to an increase in $\|\Delta P\|$. It is well understood that in a microchannel the pressure distribution is influenced by the compression effect and the rarefaction effect. In the slip regime where the rarefaction effect is relatively weak, a large θ_p results in a higher pressure gradient, and subsequently the compression effect dominates the flow so that $\|\Delta P\|$ will increase significantly with θ_p. But when the pressure ratio is small, both the rarefaction effect and compressibility effect are weak, and the nonlinear dependence of θ_p in $\|\Delta P\|$ is observed. On the whole, the increase of θ_p leads to an increase in $\|\Delta P\|$ and this influence weaken when the θ_p is larger. On the other hand, as Kn is relatively large ($\mathrm{Kn}_{out}=1.0$), the results given in Fig. 6(b) show that, although change of $\|\Delta P\|$ is similar to the result with $\mathrm{Kn}_{out}=1.0$, the increase rate of $\|\Delta P\|$ is less than that as $\mathrm{Kn}_{out}=0.1$. This is because the rarefaction effect in enhanced as Kn_{out} increases from 0.1 to 10, and the compression effect is suppressed.

4.3 Effect of aspect ratio

Besides the rarefaction and compression effects, the aspect ratio has also obvious effect to the pressure distribution of the microchannel. Actually, some previous studies on gas flow in long micro channels [7,36] and short ones have been conducted [35,37]. For examples, Maurer et al. performed some experiments with Kn=0.3 and ε=0.001 [7]; Mavriplis et al. explored the applicability of the DSMC method for supersonic and subsonic flows with varying aspect ratios, and found that the results are strongly dependent on the channel aspect ratio [37]. We now study the effect of the aspect ratio on the pressure distribution and considered cases with ε changes from 0.01 to 0.1, $\theta_p=2.0$, $\mathrm{Kn}_{\mathrm{out}}=0.03$.

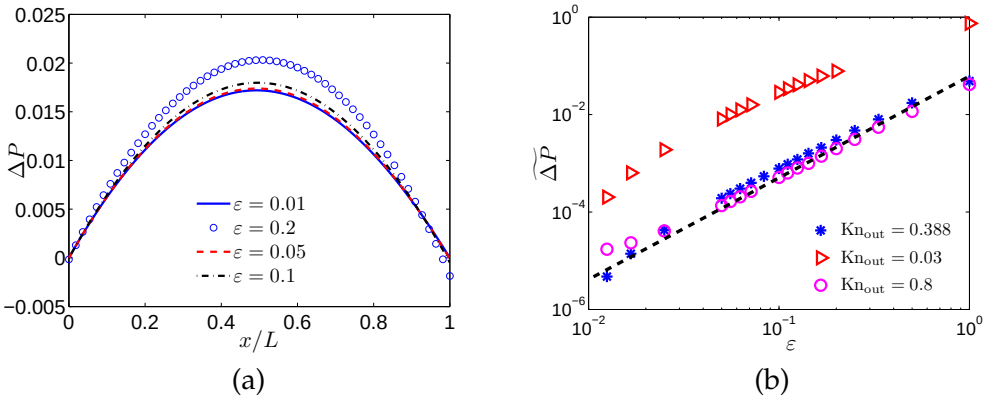

Figure 7: (a): Pressure deviations at different ε. (b): The difference between the pressure deviation with aspect ratio ε and the infinite small one.

Fig. 7 shows the pressure deviations at different aspect ratios. Fig. 7(a) indicates that the deviation increases with ε. However, in the analytical solution Eq. (2.2) and Eq. (2.4), the effect of aspect ratio ε is not included. $\widetilde{\Delta P}=\max(\Delta P(\varepsilon))-\max(\Delta P(\varepsilon_{long}))$ is also measured to indicate the vary of pressure distribution at different ε. Here we set $\varepsilon_{long}=0.01$, since the results with $\varepsilon<0.01$ are very close to those at this value. The result is shown in Fig. 7(b). It can be seen that the relationship between the nonlinear deviation of the pressure and the aspect ratio follows a power law, $\widetilde{\Delta P}=\alpha\varepsilon^{\beta}$, with $\beta\approx 2.0$ (see Table 1), $\widetilde{\Delta P}$ increases with increasing ε. This is the result of the larger compression effect due to the larger pressure gradient in a shorter channel.

Table 1: α and β with different Knudsen number.

$\widetilde{\Delta P}=\alpha\varepsilon^{\beta}$		
Kn_{out}	α	β
0.03	2.9221	1.847
0.388	0.003	2.073
0.8	$5.1642*10^{-4}$	1.831

5 Conclusions

In this work gaseous flows in microchannels with different height/length ratios are studied in both slip and transition regimes based on a MRT-LBE model. The Knudsen minimum phenomenon in mass flow rate is successfully captured. Particularly, the pressure distributions along the channel are carefully analyzed. The effects of the Knudsen number, pressure ratio, and aspect ratio are investigated. A fundamental knowledge on this effect can be summarized as follows:

First, in slip and transition regimes the increase of Knudsen number tends to diminish the curvature of the pressure distribution. It is also found that there exists a minimum in the distribution of the pressure deviation as a function of the Knudsen number, which is the result of the combined compression and rarefication effects.

Second, we found that the magnitude of the pressure deviation increases nonlinearly with the pressure ratio, and the deviation decreases with increasing Knudsen number due to the rarefication effect.

Finally, it is shown that the relationship between the pressure deviation and the aspect ratio follows a second-order power law approximately.

Pressure distribution may be also sensitive to the shape of cross section, and gaseous flows in micro channels with different cross sections will be studied in our further work.

Acknowledgments

This work is supported by the National Natural Science Foundation of China (Grant Nos. 10972087, 51125024). Z. M. Xu is grateful to Dr. G. J. Liu for her careful proofreading of manuscript.

References

[1] X. He and N. Ling, Lattice Boltzmann simulation of electrochemical systems, Comput. Phys. Commun., 129 (2000), 158–166.
[2] G. E. Karniadakis, A. Beskok and N. Aluru, Microflows and nanoflows: fundamentals and simulation, Int. Appl. Mech., (2005).
[3] S. Arcidiacono, I. V. Karlin, J. Mantzaras and C. E. Frouzakis, Lattice Boltzmann model for the simulation of multicomponent mixtures, Phys. Rev. E, 76 (2007), 046703.
[4] B. Arkilic, A. Schmidt and S. Breuer, Gaseous slip flow in long microchannels, J. Microelectromech., 6 (1997), 167–178.
[5] J. Jang and S. T. Wereley, Pressure distributions of gaseous slip flow in straight and uniform rectangular microchannels, Microfluid and Nanofluid, 1 (2004), 41–51.
[6] C. Shen, D. B. Tian, C. Xie and J. Fan, Examiation of the LBM in simulation of microchannel flow in transitional regime, Microscale Thermophys. Eng., 8 (2004), 405–410.
[7] J. Maurer, P. Tabelin, P. Joseph and H. Willaime, Second-order slip laws in microchannels for helium and nitrogen, Phys. Fluids, 15 (2003), 2613–2621.

[8] S. Varoutis, S. Naris, V. Hauer, C. Day and D. Valougeorgis, Computational and experimental study of gas flows through long channels of various cross sections in the whole range of the Knudsen number, J. Vac. Sci. Technol. A, 27 (2009), 89–100.
[9] T. Ohwada, Y. Sone and K. Aoki, Numerical analysis of the Poiseuille and thermal transpiration flows between two parallel plates on the basis of the Boltzmann equation for hard-sphere molecules, Phys. Fluids A, 1 (1989), 2042–2049.
[10] F. Verhaeghe, L. S. Luo and B. Blanpain, Lattice Boltzmann modeling of microchannel flow in slip flow regime, J. Comput. Phys., 228 (2009), 147–157.
[11] X. B. Nie, G. D. Doolen and S. Y. Chen, Lattice-Boltzmann simulations of fluid flows in MEMS, J. Stat. Phys., 102 (2002), 279–289.
[12] C. Y. Lim, C. Shu, X. D. Niu and Y. T. Chew, Application of lattice Boltzmann method to simulate microchannel flows, Phys. Fluids, 14 (2002), 2299–2308.
[13] Y. H. Zhang, R. S. Qin and D. R. Emerson, Lattice Boltzmann simulation of rarefied gas flows in microchannels, Phys. Rev. E, 71 (2005), 047702.
[14] J. F. Zhang, Lattice Boltzmann method for microfluidics: models and applications, Microfluid and Nanofluid, 10 (2005), 1–28.
[15] Z. L. Guo, T. S. Zhao and Y. Shi, Physical symmetry, spatial accuracy, and relaxation time of the lattice Boltzmann equation for microgas flows, J. Appl. Phys., 99 (2006), 074903.
[16] Z. L. Guo, C. G. Zheng and B. C. Shi, Lattice Boltzmann equation with multiple effective relaxation times for gaseous microscale flow, Phys. Rev. E, 77 (2008), 036707.
[17] C. Cercignani, Mathematical Methods in Kinetic Theory, Plenum, New York, 1990.
[18] X. Y. He and L. S. Luo, A priori derivation of the lattice Boltzmann equation, Phys. Rev. E, 55 (1997), R6333–R6336.
[19] X. Shan and X. He, Discretization of the velocity space in the solution of the Boltzmann equation, Phys. Rev. Lett., 80 (1998), 65–68.
[20] D. W. Stops, The mean free path of gas molecules in the transition regime, J. Phys. D, 3 (1970).
[21] Z. L. Guo, B. C. Shi and Ch. G. Zheng, An extended Navier-Stokes formulation for gas flows in the Knudsen layer near a wall, Euro. Phys. Lett., 80 (2007), 24001.
[22] X. Niu, S. A. Hyodo, T. Munekata and K. Suga, Kinetic lattice Boltzmann method for microscale gas flows: issues on boundary condition, relaxation time, and regularization, Phys. Rev. E, 76 (2007), 036711.
[23] Y. H. Zhang, X. J. Gu, R. W. Barber and D. R. Emerson, Capturing Knudsen layer phenomena using a lattice Boltzmann model, Phys. Rev. E, 74 (2006), 046704.
[24] M. Fichman and G. Hetsroni, Viscosity and slip velocity in gas flow in microchannels, Phys. Fluids, 17 (2005), 123102.
[25] D. A. Lockerby, J. M. Reese and M. A. Gallis, Capturing the Knudsen layer in continuum-fluid models of non-equilibrium gas flows, AIAA J., 43 (2005), 1391–1393.
[26] X. Shan, X.-F. Yuan and H. Chen, Kinetic theory representation of hydrodynamics: a way beyond the Navier-Stokes equation, J. Fluid Mech., 550 (2006), 413–441.
[27] S. K. Loyalka, N. Petrellis and T. S. Strovick, Some numerical results for the BGK model: Thermal creep and viscous slip problems with arbitrary accomodation at the surface, Phys. Fluids, 18 (1975), 1094–1099.
[28] X. Nian, E. John and A. Tim, Microtube gas flows with second-order slip flow and temperature jump boundary conditions, Proc. 4th Inter. Conf. on Nanochannels, Microchannnels, and Minichannels, Parts A and B, (2006), 385–393.
[29] Y. Zhou, R. Zhanga, I. Staroselsky, H. Chen, W. T. Kim and M. S. Jhon, Simulation of micro-

and nano-scale flows via the lattice Boltzmann method, Phys. A, 362 (2006), 68–77.
[30] M. Darbandi and Y. Daghighi, Computation of rarefied gaseous flows in micro to nano scale channels with slip to transient regimes using general second-order quadratic elements, Proc. 6th Int. Conf. nanochannels, Microchannels and Minichannels, (2008), 55–64.
[31] S. H. Kim, H. Pitsch and D. B. Iain, Slip velocity and Knudsen layer in the lattice Boltzmann method for microscale flows, Phys. Rev. E, 77 (2008), 026704.
[32] Z. P. Duan, Second-order gaseous slip flow models in long circular and noncircular microchannels and nanochannels, Microfluid and Nanofluid, 5 (2012), 805–820.
[33] S. Succi, Mesoscopic modelling of slip motion at fluid-solid interfaces with heterogeneus catalysis, Phys. Rev. Lett., 89 (2002), 064502.
[34] S. Ansumali and I. V. Karlin, Kinetic boundary conditions in the lattice Boltzmann method, Phys. Rev. E, 66 (2002), 026311.
[35] C. Shen, J. Faa and C. Xie, Statistical simulation of rarefied gas flows in micro-channels, J. Comput. Phys., 189 (2003), 512–526.
[36] S. Colin, Rarefaction and compressibility effects on steaty and transient gas flow in microchannels, Microfluid and Nanofluid, 1 (2005), 268–279.
[37] C. Mavriplis, J. C. Ahn and R. Goulard, Heat transfer and flow fields in short microchannels using direct simulation monte carlo, AIAA J. Thermophys., 11 (1997), 489–496.